Coupled Organic−Inorganic Nanostructures with Mixed Organic Linker Molecules

Florian Grassl, Aladin Ullrich, Ahmed E. Mansour, Shaimaa M. Abdalbaqi, Norbert Koch, Andreas Opitz, Marcus Scheele, and Wolfgang Brütting*

ABSTRACT: The electronic properties of semiconducting inorganic lead sulfide (PbS) nanocrystals (NCs) and organic linker molecules are dependent on the size of NCs as well as the used ligands. Here, we demonstrate that a weakly binding ligand can be successfully attached to PbS NCs to form a coupled organic−inorganic nanostructure (COIN) by mixing with a strong binding partner. We use the weakly binding zinc β-tetraaminophthalocyanine (Zn4APc) in combination with the strongly binding 1,2-ethanedithiol (EDT) as a mixed ligand system and compare its structural, electronic, and (photo-)electrical properties with both

mixing of ligands   ligand exchange

single-ligand COINs. It is found that binding of Zn4APc is assisted by the presence of EDT leading to improved film homogeneity, lower trap density, and enhanced photocurrent of the derived devices. Thus, the mixing of ligands is a versatile tool to achieve COINs with improved performance.

KEYWORDS: semiconductor nanocrystals, PbS nanocrystal solid, coupled organic−inorganic nanostructures, ligand exchange, mixed ligands, phthalocyanine

1. INTRODUCTION

Coupled organic−inorganic nanostructures (COINs) are composed of semiconducting inorganic nanocrystals (NCs) and organic semiconductor molecules covalently coupled to the surface of the NCs.[1] COINs utilize these organic molecules as cross-linking agents to facilitate charge transport between the NCs. COINs have large carrier mobilities with ≈10^{-2} cm^2/(V s),[2,3] size-tunable band gaps[4,5] with NC sizes typically in the range of 1−20 nm in diameter,[6] and the potential to harvest sunlight in the visible and near-infrared regime.[7,8] They additionally offer the perspective to combine efficient carrier transport with a high degree of structural order.[9] Proper alignment of the energy levels of both species allows for implementation into field-effect transistors[10,11] or solar cells.[12] A well-known organic ligand is 1,2-ethanedithiol (EDT), especially with PbSe and PbS NCs.[5] However, this ligand has the drawback of being very short (≤0.6 nm) as compared to the native oleic acid (OA) ligands (≈1.9 nm) that are typically used to stabilize these colloidal particles in solution.[13] Upon ligand exchange in films, this leads to extreme shrinkage of interparticle distances and, thus, non-ideal film morphology as will be shown later.

In this work, we study zinc β-tetraaminophthalocyanine (Zn4APc) as a ligand,[14] which has a size (≈1.7 nm) comparable to OA. Moreover, Zn4APc is a π-conjugated molecule such that it can be expected to contribute to light absorption and, thus, enable its use in opto-electronic devices[14]
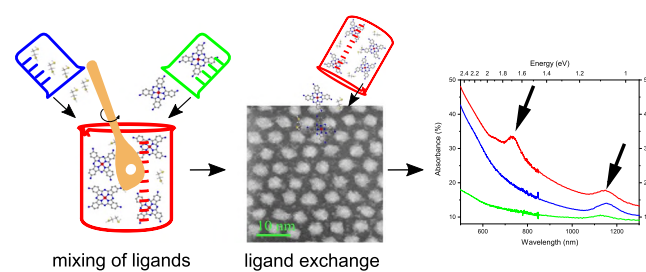
with lead sulfide (PbS) NCs. We compare Zn4APC COINs to EDT COINs[5] with respect to film formation and structure as well as optical and electrical properties. We find that sufficient binding (between the ligand and PbS) and useful COIN film quality are only possible if a mixture of EDT and Zn4APc ligands is used. This is an important precondition for the application of these materials in devices.

2. EXPERIMENTAL SECTION

2.1. Sample Preparation/Device Fabrication. Glas substrates coated with 90 nm indium−tin oxide (ITO) were purchased from Thin Film Devices (U.S.A.) and prestructured field-effect transistor (FET) substrates for dark conductivity measurements were from IPMS Dresden (Germany). Conventional carbon-coated copper grids (type S160-3) from Plano (Germany) were used for scanning transmission electron microscopy (STEM) measurements. Clevios^{TM} PEDOT:PSS was purchased from Heraeus Clevios GmbH (Germany), BCP was from Sigma-Aldrich (U.S.A.), and C$_{60}$ from Lumtec (Taiwan). PbS NCs were purchased from Quantum Solutions (Saudi Arabia) with 10 mg/mL solution in octane; Zn4APc was

synthesized by a previously reported method.[14,15] EDT was purchased from Sigma-Aldrich.

All substrates were cleaned in an ultrasonic bath for 10 min each in technical acetone, pure acetone, and pure isopropanol and then blow-dried. PEDOT:PSS was spin-coated from an aqueous dispersion and subsequently dried at 125 °C. Bathocuproine (BCP), fullerene (C_{60}), and the metal cathodes were all evaporated in UHV ($<5 \times 10^{-7}$ mbar).

COIN preparation was carried out in a nitrogen glovebox under O_2/H_2O-free conditions. PbS solutions were further diluted with 72 μL of PbS in 1080 μL of n-hexane. For the EDT ligand, 36 μL of EDT was dissolved in 47 mL of acetonitrile, and the dipping step was 30 s. For the Zn4APc ligand, 15 mg of Zn4APc was dissolved in 50 mL of acetonitrile and the dipping step was 180 s. The dynamic process of ligand exchange in solution depends on multiple parameters like the concentration of ligands or the exposure time.[16,17] For the 1:1 mixture of both ligands, a compromise between the rapid ligand exchange of EDT (30 s) and the unsuccessful trial of the neat Zn4APc ligand solution was used. For this mixture, an exposure time of 180 s turned out to yield good results. Sample transfer for further evaporation steps was carried out under O_2/H_2O-free conditions.

2.2. Instrumentation. Scanning transmission electron microscopy (STEM) was performed on a JEOL Neoarm F200 with a cold field-emission gun (Cold FEG), operated at 200 keV electron beam energy under vacuum. The image for PbS−OA ligands showed a small drift and was calibrated using the lattice constants. Atomic force microscopy (AFM) was performed on a dimension icon scanning probe microscope (Bruker) under an ambient atmosphere. Photoelectron spectroscopy was performed using a hemispherical analyzer EA125 (Scienta Omicron GmbH) with an energy resolution of 130 meV. X-ray photoelectron spectroscopy (XPS) was performed using a non-monochromatic Mg Kα radiation (1253.6 eV), while ultraviolet photoelectron spectroscopy (UPS) was performed using He I radiation (21.22 eV) from a gas discharge lamp. He I radiation was attenuated by passing through an aluminum foil (350 nm) before reaching the sample to minimize sample damage. The spectra were collected using a pass energy of 2.0 eV for UPS as well as 20 and 50 eV for high-resolution and survey XPS scans, respectively. The energy resolution and energy scale calibration were determined by measuring the Fermi edge of a clean Au crystal. The secondary electron cutoff (SECO) was measured at a sample bias of −10 V. Samples were transferred to the UHV chamber without exposure to the ambient atmosphere. Absorption measurements were performed by an Ellipsometer (Sentech SE850). Profilometer measurements were done with a DEKTAK 8 from Veeco. Both measurements were performed under an ambient atmosphere. The dark conductivity samples were characterized using a Keithley 4200 Semiconductor Parameter Analyzer in a cryostat under a vacuum. The photodiodes were characterized electrically by recording current−voltage (J−V) characteristics using a source measure unit (Keithley 236 SMU). The currents were measured in the dark and under one sun-simulated AM1.5G, 100 mW/cm^2 illumination with a Xe lamp (Oriel 300 W with AM1.5G filters) integrated into a glovebox system under a nitrogen atmosphere. The illumination intensity was referenced against a calibrated silicon reference cell. Incident photon-to-current efficiency (IPCE) measurements were carried out under monochromatic illumination (Omni-λ300 Monochromator/Spectrograph, Zolix Instruments Co., Ltd.) and lock-in detection. Photodiode measurements were performed under a nitrogen atmosphere. The transport for dark conductivity and photodiode measurements were carried out under O_2/H_2O-free conditions. To estimate the length of the ligands, we performed a simple force-field optimization in a vacuum with the OPLS3 Force Field[18] and MacroModel as a part of the Schrödinger Materials Science Suite.[19] After the simulation, we determined the average distance between the end groups of the ligands.

2.3. COIN Preparation. COINs consisting of PbS NCs and Zn4APc or EDT as ligands are prepared from the starting materials. Initially, the PbS NCs with a diameter of 3.7 nm are OA-capped and suspended in octane. Their first excitonic absorption peak maximum is at about 1090 nm; thus, they have an optical gap of about 1.13 eV.

For the preparation of thin-film COINs, a dip-coating process was used in a glovebox under a nitrogen atmosphere.[20] Therein, the native OA ligands of each monolayer of deposited PbS NCs are exchanged with bi- or tetra-dentate new ligands to cross-link NCs and thus form a coupled organic-inorganic layered system. This step is repeated several times to achieve the desired film thickness. Visualization of this process is shown in the Supporting Information, Figure S1.

In detail, prior to the start of the whole deposition process, the pristine colloidal PbS NC suspension is further diluted in n-hexane and stirred at room temperature for 1 h. Ligand molecules—EDT, Zn4APc, or a mixture of both at a 1:1 ratio—were dissolved in acetonitrile and stirred at 50 °C for 12 h on a hotplate. Then, the first coating step is the dipping of the substrate (glass, glass coated with ITO, or Si wafers with an oxide layer) into the ligand container for a certain time (depending on the ligand) and drying for 30 s under a nitrogen atmosphere. This initial ligand coverage serves as a seed layer on which the PbS NCs preferentially attach.[21] The next step consists of dipping the substrate into a container with PbS NCs for 30 s and drying in a nitrogen atmosphere for another 30 s before dipping again into the container with ligands. In this step, the ligand exchange takes place. Ideally, all of the native OA ligands are replaced by the organic linker molecules. After drying for 30 s, the last dipping is performed in a container with the solvent acetonitrile to wash away excess (nonbinding) ligands, OA, and PbS NCs. Thereafter, the samples are heated at 100 °C on a hotplate for at least 5 min to dry the film and to avoid contamination of the next container. Subsequently, these steps are repeated, but without the first ligand dipping step, until the desired thickness is reached. Typically, we used four repetitions to get an overall COIN film thickness of around 50 nm, except for the STEM samples, which were dipped only once for just 10 s to yield a monolayer. Finally, all samples were heated in a vacuum oven (10^{-3} mbar) in the glovebox at 100 °C for 16 h to get rid of the remaining solvents, the potential residual oxygen, and water.

The decisive step for successful COIN preparation is the ligand exchange (Figure 1). This occurs in the liquid phase, where one has a dynamic equilibrium between attachment and detachment of ligands. For monodentate ligands, like OA, this means that the ligand shell
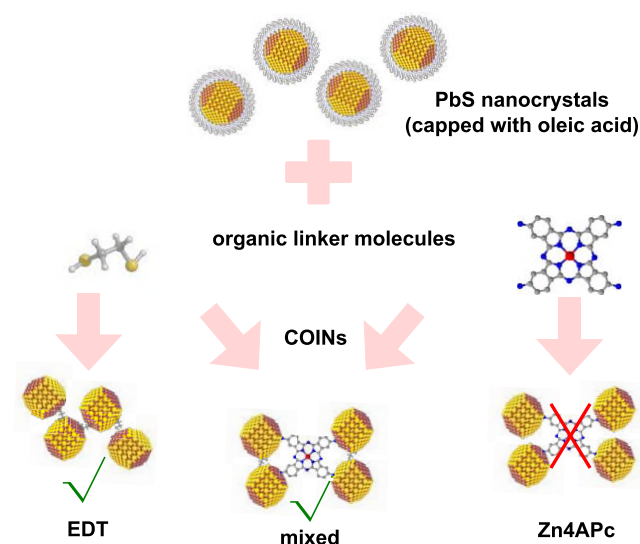

Figure 1. Visualization of the ligand exchange process. The native OA shell of the PbS NCs is replaced by organic linker molecules with two (EDT) or four (Zn4APc) anchoring groups, thus leading to coupled organic−inorganic nanostructures (COINs) of different extensions and regularities, as discussed further below. The checkmarks and the cross clarify the reality. The sketch of the PbS nanocrystal is reproduced from the original publication by Scheele et al.[41] Copyright 2014 American Chemical Society.

around PbS nanocrystals is not densely packed and offers sites for stronger binding groups. This is the case for thiol groups as with EDT. Furthermore, EDT is a bidentate ligand, which is able to cross-link PbS NCs or pin them to the substrate. For Zn4APc, it is known that the amino group is not binding very strongly.[22,23] However, due to four binding sites some kind of chelating effect might promote ligand exchange, as it was reported for the related Cu4APc ligand.[24]

3. RESULTS AND DISCUSSION

The main focus of this manuscript is to study the binding behavior of the different ligands to PbS NCs and their effect on COIN-film morphology as well as device performance. Scanning transmission electron microscopy (STEM) is used to examine the local structure of different COINs, whereas atomic force microscopy (AFM) is used to image the surface morphology. Furthermore, ultraviolet photoelectron spectroscopy (UPS), X-ray photoelectron spectroscopy (XPS), and optical absorption measurements are used to characterize the electronic properties of COINs. In the end, devices (photodiodes and field-effect transistors) are fabricated to investigate the resulting optoelectronic properties.

3.1. Layer Structure. For a deeper understanding of the binding of PbS NCs with different ligands, STEM measurements of monolayers deposited on carbon-coated transmission electron microscopy (TEM) grids were performed. Figure 2 shows the structure of COINs with different ligand systems, including (a) the native PbS NCs capped with OA, (b) COINs with EDT, (c) COINs with Zn4APc, and (d) COINs with a mixture of both ligands. Further details are given in the Supporting Information, Figures S2−S9 as well as Tables S1 and S2.

The native OA-capped PbS NCs arrange in a hexagonal close-packed layer, typical for weakly interacting particles. The ligand-capped NCs have a 3.7 nm inorganic core and a 1.9 nm thick ligand sphere (see the Supporting Information, Figures S2 and S3 for more details). Also shown is an inset with the lattice structure of a single PbS NC, from which the preferred orientation and the lattice constants are obtained. There are some areas without PbS NCs in this highly regular monolayer arrangement. Note that there is apparently some debris visible in the noncovered areas. These are probably tiny pieces of elementary lead, stemming from the PbS NC production process itself or during the film preparation.

For COINs with EDT as ligand, the structure changes completely as the hexagonal close-packed arrangement disappears. The PbS NCs rather form clusters with a very small distance to each other. According to simulations with Schrödinger's Materials Science Suite, the length of an EDT molecule is 0.58 nm; however, the actual distance is hardly measurable within the arrangement of the particles as the PbS NCs have almost merged. The reported values in the literature range between 0.2[20] and 0.25 nm,[25] in agreement with our observation. These small distances can be understood by the elimination of the two terminal hydrogen atoms of the EDT ligand upon the formation of the covalent linkage between two PbS NCs. On the other hand, this particle clustering leads to large uncovered areas on the substrate due to the drastic shrinkage of the interparticle distance upon ligand exchange with the short EDT molecule and the lack of further PbS NCs to fill the resulting voids.

For COINs with Zn4APc as a ligand, the arrangement of the particles looks similar to the OA case in the monolayer region of the respective image. The STEM image for the 100 nm scale
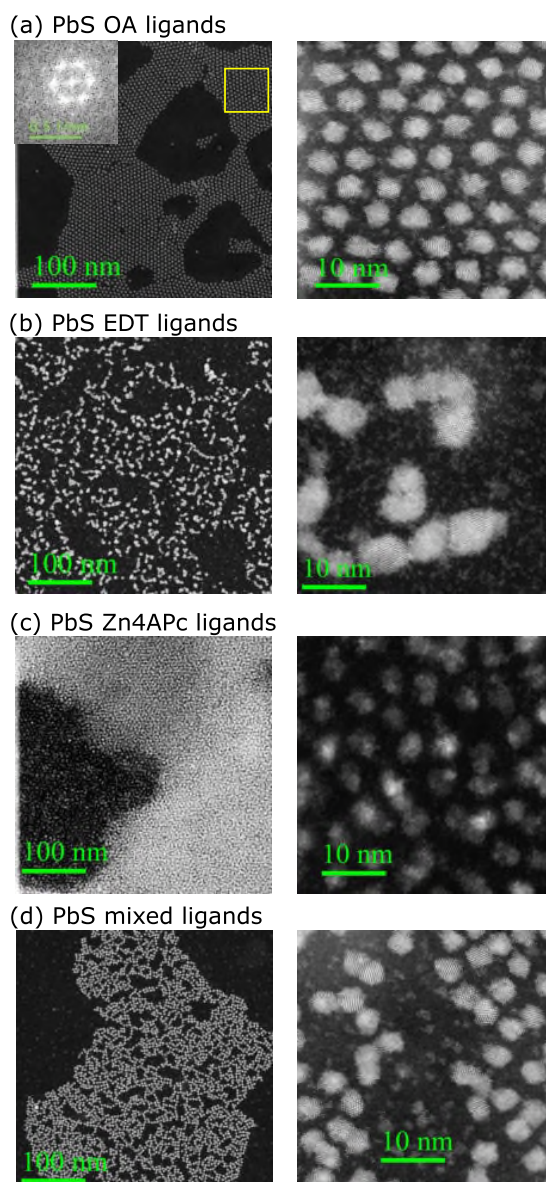
(a) PbS OA ligands

(b) PbS EDT ligands

(c) PbS Zn4APc ligands

(d) PbS mixed ligands

Figure 2. Scanning transmission electron microscopy images of PbS NCs before (a) and after ligand exchange (b−d). The left column gives an overview (scale bar: 100 nm), whereas the right column zooms into a characteristic region of each image (scale bar: 10 nm). For OA ligands, a sixfold symmetry is obtained from the fast Fourier transform (FFT) analysis, represented in (a). For Zn4APc ligands, the 100 nm scale image indicates more than a monolayer in the bright area, while the 10 nm image was taken from the monolayer region (dark area).

indicates more than a monolayer in the bright area; for further analysis, only the monolayer region was used. There are basically no PbS free areas and a relatively homogeneous distribution but the hexagonal arrangement is strongly disturbed. From the analysis of interparticle distances (see the Supporting Information, Figures S4 and S7 and Table S1), we obtain a value of about 1.9 nm, identical to the native OA-capped PbS NC layer. However, since the simulated length of Zn4APc (including the terminal amino groups) is only about 1.74 nm, and literature values for Cu4APc, a very similar ligand, are even shorter with numbers between 1.3 and 1.5 nm,[14,24] we suppose that the Zn4APc does not bind to PbS

NCs in this case. In addition, multilayers are formed, which are not analyzed further.

Finally, the COINs with mixed ligands have an arrangement with both large interparticle distances as it should be in the COINs with the Zn4APc case (simulation and compared literature values) and clustered particles found for COINs with EDT. This gives an indication that both ligands are bound to PbS NCs in this case. However, the merging behavior is not visible as with the EDT ligands alone and is rather a formation of dimers and trimers. On a larger scale, one can even identify linear chains and cubic arrangements of NCs. Again, due to the shrinkage of the average interparticle distance, some uncovered regions are formed. However, in a thicker film, one can expect that these voids are filled by subsequent layers. The average distance obtained from the analysis of interparticle distances is 1.30 nm.

Recapitulating from these STEM images, it is possible to understand the binding behavior between NCs and ligands. The OA and Zn4APc ligands have similar binding behaviors and distances between the NCs; thus, it seems that Zn4APc is not binding. For EDT ligands the PbS form clusters with a very small NC distance. The mixed ligands appeared to have EDT and Zn4APc ligands binding behavior.

The orientation of the particles itself is influenced additionally by the substrate.[26] A summary of structural parameters obtained from a fast Fourier transform (FFT) analysis is given in the Supporting Information, Tables S1 and S2.

3.2. Film Morphology.
For additional information about the morphology of thicker films, AFM measurements were performed (see Figure S10 in the Supporting Information). These samples were coated four times resulting in a thickness of about 50 nm.

The native OA-capped PbS NC film has the smoothest surface with a root-mean-square (RMS) roughness of 1.90 nm. A similar value is obtained for Zn4APc COINs with an RMS of 1.97 nm. The EDT COINs show island formation with peak heights up to 30 nm and an RMS of 3.37 nm. This is the roughest surface of all used COINs. The mixed COINs are in between these values with an RMS of 2.43 nm.

Thus, AFM images confirm the view that ligand exchange with EDT leads to film inhomogeneities because the interparticle distance shrinks drastically, which is accompanied by large surface roughness. The ligand exchange with Zn4APc leads to almost identical RMS as the native PbS NCs; once more, this could indicate that there was no ligand exchange at all. On the other hand, the intermediate roughness of the mixed ligand COINs seems to indicate that at least some degree of ligand exchange has occurred.

3.3. Optical Properties.
To get more insights into the composition of different COINs, optical absorption measurements were performed. The native OA-capped PbS NCs in solution show a first excitonic absorption peak maximum at about 1090 nm (Figure 3, right axis), which leads to an energy gap of 1.13 eV. According to Moreels et al., the corresponding NC size is 3.7 nm,[27] in good agreement with the STEM images. Also shown on the same axis is the absorption of the Zn4APc ligands in solution having two characteristic absorption peak maxima at about 630 and 700 nm.

The absorption spectra across the Vis and NIR range for the different COINs are shown on the left axis of Figure 3. For COINs with EDT ligands, the absorption decreases with increasing wavelength and shows only one pronounced peak at
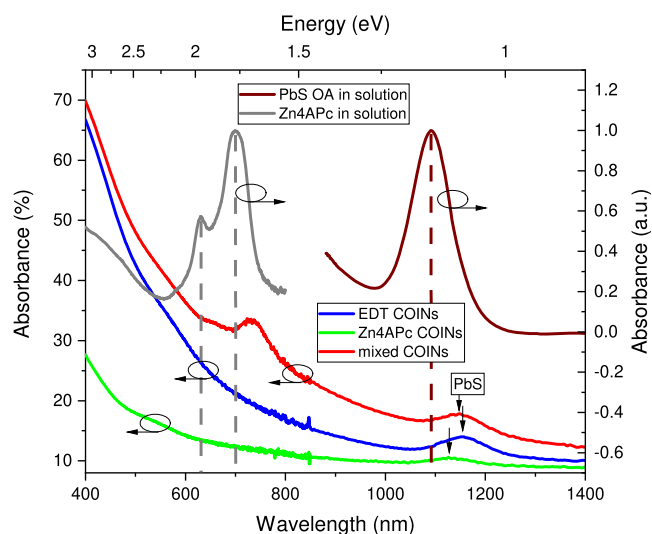

Figure 3. Optical absorption measurements for the native OA-capped PbS NCs and the Zn4APc ligands in solution (right axis) as well as absorption measurements of films of COINs with different ligands (left axis). The excitonic peak for the native PbS NCs in solution at about 1090 nm is redshifted in films of COINs with different ligands: 1150 nm (EDT), 1130 nm (Zn4APc), and 1145 nm (mixed).

about 1150 nm. This corresponds to the absorption peak of PbS NCs. The redshift of 60 nm compared to the native colloidal solution is caused by a solid-state shift and the use of a different ligand than OA. Due to the nonconjugated nature of EDT, however, there is no additional peak in the investigated range coming from the ligand. COINs with the Zn4APc ligand show only a hardly noticeable absorption peak at 1130 nm. The expected ligand peaks in the visible range are not detectable. This indicates that there are no (or very few) Zn4APc ligands attached to PbS NCs in the sample. The mixed COINs show both the absorption peak for PbS NCs at 1145 nm (again redshifted by about 55 nm in comparison to the solution) as well as the peaks of the Zn4APc ligands appearing at 680 and 720 nm, which indicates a redshift of 20−30 nm in comparison to the Zn4APc ligand solution alone. This shows that Zn4APc ligands are bound to PbS NCs and absorption in the visible and NIR range is significantly improved with the mixed ligands.

In Section 3.7, the shift of the absorption peaks will be discussed further in relation to the effective values of the dielectric constant.

3.4. Energy Levels.
Photoelectron spectroscopy was performed on multilayer films deposited on ITO substrates to measure the energy levels (valence level (VL) and work function by UPS) of COIN films with different ligands as well as the chemical composition of the films (by XPS). UPS is used to measure the occupied density of states and can accordingly be used to deduce the valence level with respect to the Fermi level (low-binding energy onset). In addition, the work function can be obtained from the secondary electron cutoff (SECO), which is given by the onset of the spectrum at high binding energy. The work function is defined as the energy difference between the Fermi level and the vacuum level of the film.

Figure 4a shows the secondary electron cutoff of the four different samples (together with a bare ITO substrate as reference) with the energy scale converted to the resulting work function. The work function is determined by the low-
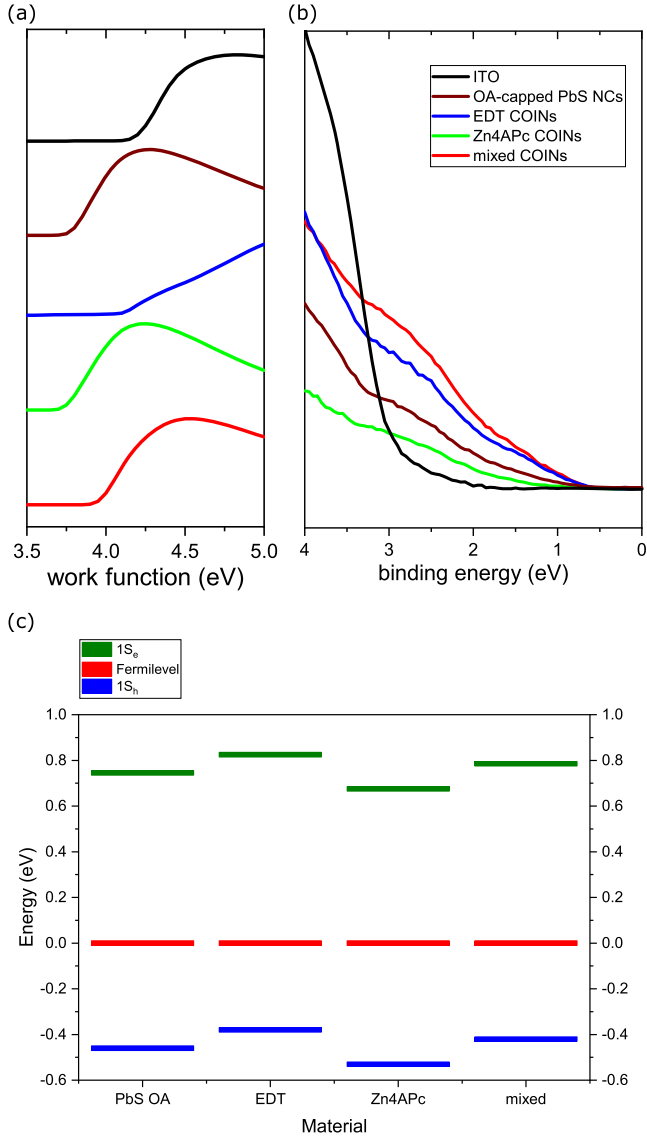
Figure 4. (a) Measured secondary electron cutoff of different samples; the onset energy yields the respective work function. (b) UPS spectra of the low binding energy region of each sample, from where the valence level onset is determined; details are in the Supporting Information. (c) The resulting energy level diagram of PbS COINs with different ligands relative to the respective Fermi level of each sample. The energies of the $1S_h$ levels were taken from UPS measurements. For all samples, the same optical energy gap of 1.13 eV and an exciton binding energy of 0.08 eV were used to calculate the energy of the $1S_e$ level.

Figure 4b shows the valence level of different samples (binding energy with respect to the Fermi level). The VL onset (corresponding to the $1S_h$ level of PbS NCs) is obtained from an extrapolation of the curves to the instrumental background, as indicated in the SI. These values are listed in Table 1 with a negative sign because they are below the Fermi level.

Table 1. Energy Levels of COINs with Different Ligands Relative to the Fermi Level, together with the Work Functions of Different Samples

PbS + ligand	VL (eV) ≡ $1S_h$	CL (eV) ≡ $1S_e$
OA	−0.46	0.75
EDT	−0.38	0.83
Zn4APc	−0.53	0.68
mixed	−0.42	0.79

The energy of the $1S_e$ level, i.e., the conduction level (CL), of PbS NCs is calculated by adding the optical gap, obtained from absorption measurements (first excitonic absorption peak maximum), and the exciton binding energy to the VL

$$E_{CL} = E_{VL} + E_g^{opt} + 1.786 \frac{e^2}{4\pi\epsilon_0\epsilon_{QD}R} \qquad (1)$$

where the latter term represents the exciton binding energy with e for the elementary charge, ϵ_0 is the permittivity of free space, $\epsilon_{QD} \approx 18.5$ is the dielectric constant of the quantum dot (see Section 3.7 for a discussion of effective values), and R is its radius (1.85 nm).[4,29,30] The resulting values are given in Table 1, and Figure 4c shows the levels (again with respect to the Fermi level of each sample). It should be kept in mind that these exciton binding energies for quantum dots are very small (some 10 meV),[31] and, for a first-order approximation, it would be sufficient to add the optical band gap to the valence band due to uncertainty of around 0.15 eV for the UPS. For organic materials, the exciton binding energies can be much higher (1 eV)[32] and cannot be ignored to calculate the lowest unoccupied molecular orbital (LUMO) or conduction level. For COINs, the value is intermediate between these extremes, as will be discussed in Section 3.7.

XPS measurements (shown in the Supporting Information, Figures S11−S15) detect some residual indium signal for all materials, owing to the ITO substrate, but the Pb and S signals are clearly dominant. Unfortunately, the content of Zn is probably less than 1 % and thus it is below the detection limit.

3.5. Electrical Transport. The electrical transport properties of different COINs are assessed by dark conductivity and photocurrent measurements. For the dark conductivity, a field-effect transistor configuration was used. The conductance is obtained from the drain voltage sweep without the applied gate voltage (see Figure 5a). For EDT COINs, it is about 5×10^{-2} S/m while the mixed ligand COINs yield a much lower value of only 7×10^{-7} S/m. The measurement for the Zn4APc ligand alone shows just a constant current offset of about 10^{-11} A, which can be ascribed to a parasitic leakage current. The transfer characteristics for gate voltage modulation are shown in Figure 5b. Basically, it confirms the huge difference in conductivity between EDT and mixed ligand COINs as well as the absence of any nonvanishing conduction for the Zn4APc ligand alone. It also shows that both the EDT and mixed COINs are n-type; however, the EDT sample cannot be switched off, even if the gate voltage is swept to −80 V.

energy onset in the diagram. In general, bare ITO has the highest work function (4.20 eV), while all of the COINs exhibit lower values (see Table S3 in the SI). In detail, EDT COINs have a work function of 4.10 eV close to ITO, mixed ligand COINs with 3.95 eV are between EDT and OA-capped PbS (3.77 eV), and Zn4APc COINs have the lowest value with 3.73 eV. However, these values have to be taken with some care because film roughness and potentially incomplete substrate coverage can lead to artifacts, where an effective work function is obtained consisting of contributions from the film and substrate.[28] Detailed UPS and XPS spectra for different COINs are shown in the Supporting Information, Figures S11−S15.
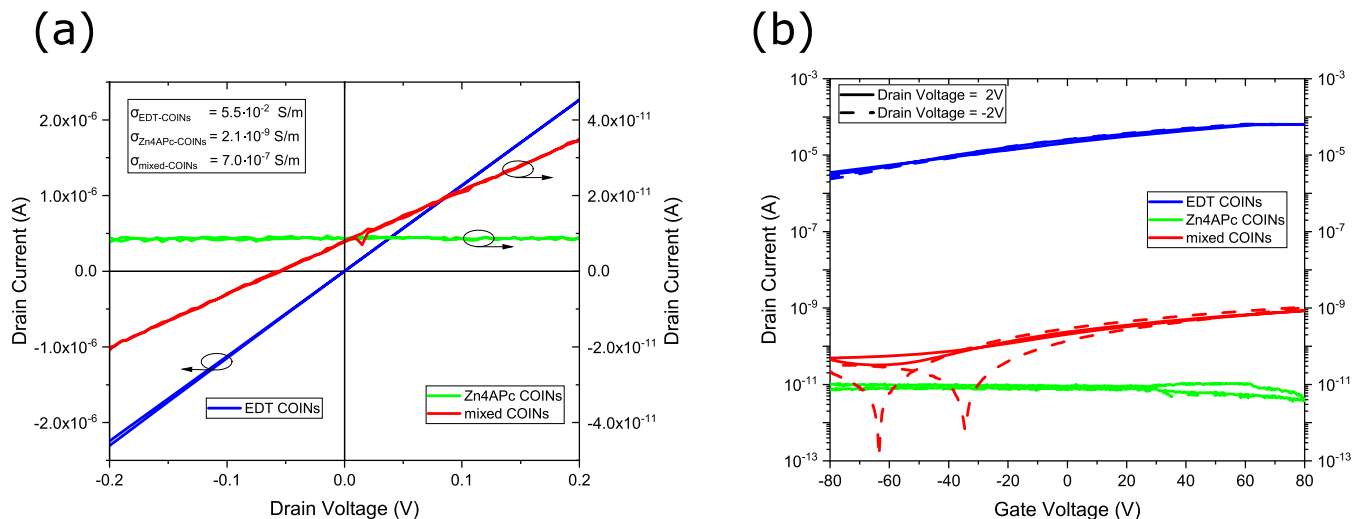
Figure 5. (a) Dark conductivity measurements without an applied gate voltage for different COINs. The current for the neat Zn4APc COINs is voltage-independent and, thus, limited by leakage. The calculated conductivity values are shown in the inset (the channel length is 2.5 μm, the channel width is 10 mm, and the thickness is 50 nm). The left and right axes have different scales. (b) Gate-voltage sweeps in the linear transistor regime for two different drain voltages. The EDT COINs cannot be switched off in the gate voltage range shown. The Zn4APc COINs have a constant very low current.

The high conductivity of the EDT COINs is caused by the extremely short interparticle distances due to the very short length of the ligand itself, allowing for efficient carrier tunneling between the PbS NCs.[2] For the Zn4APc COINs, this distance is five times higher (similar to OA ligands), which prevents a significant tunneling current. Only when EDT and Zn4APc are mixed, one finds a still low but measurable current. Furthermore, the carrier density of the different samples may also be different. The "always-on" behavior of the EDT COINs indicates that this film has a relatively high carrier density due to unintentional defect-based doping at the interface to the organic field-effect transistor (OFET) substrate.

3.6. Photodiodes. For photocurrent measurements, photodiodes were fabricated. Their general structure (inset in Figure 6b) consisted of 90 nm indium−tin oxide (ITO), 30 nm PEDOT:PSS for hole injection,[33,34] 50 nm COINs with different ligands, 50 nm fullerene (C_{60}) as an electron transport layer, 5 nm bathocuproine (BCP) as an exciton-blocking layer,[35] and 100 nm aluminum as a cathode.

The current−voltage characteristics are shown in Figure 6a,b, and device-relevant parameters are listed in Table 2. The highest photovoltage is found for a C_{60}-only reference device that does not include any COINs; however, this device has the lowest photocurrent because it lacks absorption at longer wavelengths (see below). Among the three devices with PbS COINs, the mixed ligands yield the highest photocurrent and, at the same time, also the highest photovoltage. Additionally, the slope for the mixed COINs for negative voltage in the saturation current regime is the lowest, indicating the least leakage among all three.

To get further insights, the spectral dependence of the photocurrent was measured and converted into the incident-photon-to-current efficiency (IPCE); see Figure 6c,d. It allows separating the different contributions of PbS NCs and organic ligands. For the C_{60} reference photodiode, the spectrum resembles the absorption of C_{60} with a significant peak at around 450 nm and a small shoulder at about 620 nm. All other samples have a significantly broader peak at short wavelengths owing to the additional contribution of COINs.

For EDT COINs, one finds the excitonic PbS NC peak at about 1170 nm as well as a broad featureless increase toward shorter wavelength, starting at around 1000 nm and finally merging with the C_{60} absorption peak at 615 nm. In the case of Zn4APc COINs, the IPCE spectrum follows the same overall trend but it exhibits an additional double-peak structure between 700 and 800 nm; however, as compared to the absorption spectrum of Zn4APc in solution, where the 720 nm peak is dominant, there is a second redshifted peak of almost equal height close to 800 nm. In analogy to ZnPc films, this may tentatively be assigned to aggregates of ligand molecules that are not bound to PbS NCs. On the other hand, for the mixed ligand COINs, one finds the typical signature of nonaggregated Zn4APc ligands with the main peak at 720 nm and a smaller one at about 650 nm. Remarkably, the mixed ligand system has the highest IPCE over the whole spectral range, in agreement with the highest short-circuit current of all photodiodes.

When plotted on a logarithmic scale (see Figure 6d), one can further notice a difference in the so-called subgap slope of the photocurrent, i.e., at energies below the excitonic absorption peak of PbS at about 1.1 eV. In this range, exponential decay of the IPCE spectrum can be observed, which is characterized by an Urbach energy E_U that can be obtained from the slope of a linear fit.[36,37] It is a measure for the steepness of a semiconductor's band edge, which is often found to be broadened by tail states that originate from disorder within the material.[38] The higher the value of E_U, the higher is the degree of disorder.[38] Interestingly, EDT COINs have a much shallower photocurrent decay and, thus, a higher Urbach energy of 44.8 meV than Zn4APc (28.3 meV) and mixed COINs (25.8 meV). This could be another hint for a higher defect density in the EDT case, in agreement with the dark conductivity measurements.

3.7. Discussion. Ligand exchange is a well-established technique to tune the electronic properties of thin-film assemblies of semiconductor NCs, like the here studied colloidal PbS NCs that are natively terminated with insulating OA molecules after the film preparation.[31,39] A widely used
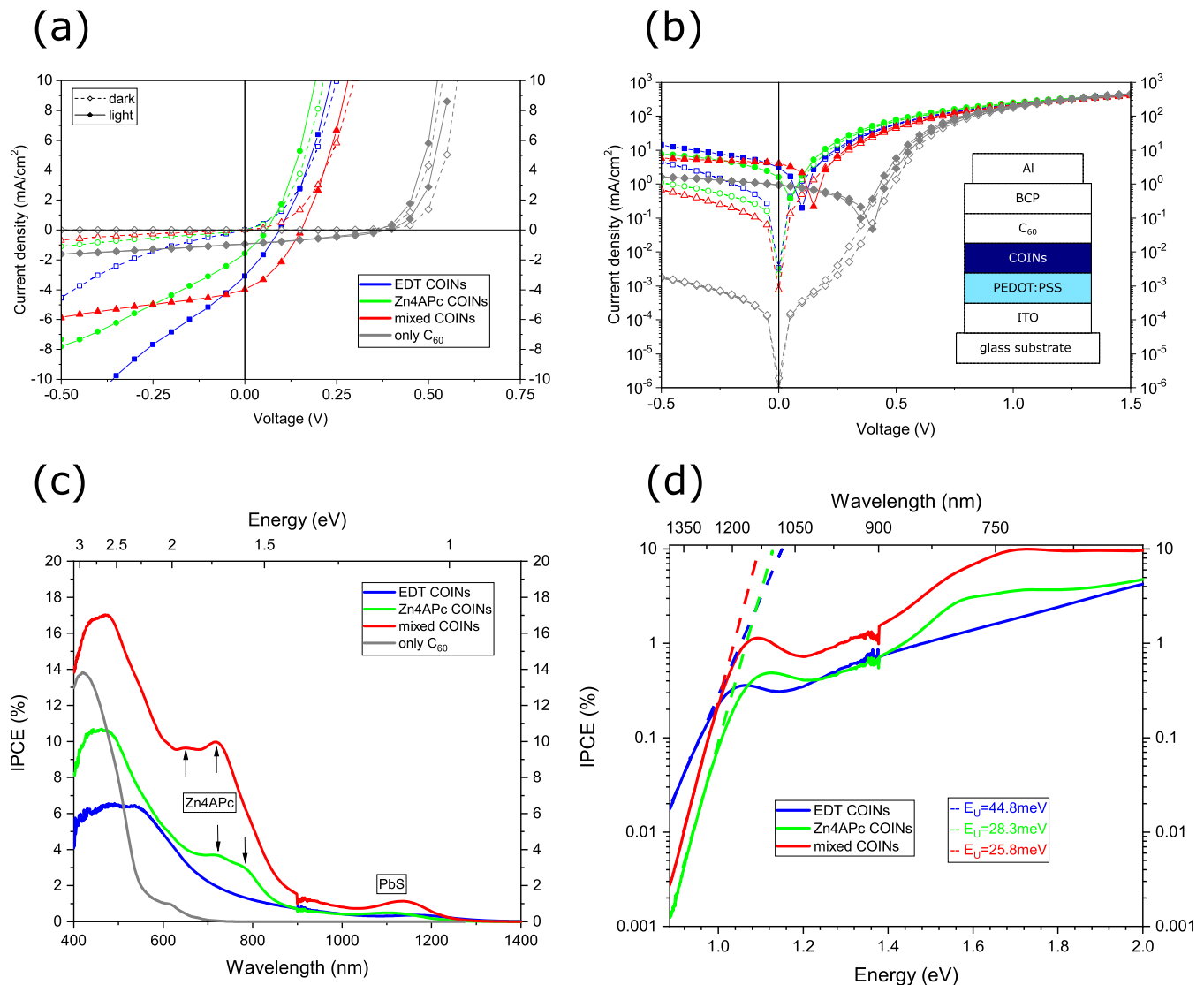
Figure 6. (a, b) Electrical device characteristics for the three different ligands without illumination and with simulated sunlight. (a) the current−voltage characteristic on (a) linear and (b) on a logarithmic scale. Also shown in (b) is the sample stack for these photodiodes. (c, d) Incident photon-to-current conversion efficiency, i.e., the external quantum efficiency of the photodiodes under short-circuit conditions with variable monochromatic illumination plotted on linear (c) and logarithmic (d) scale. (d) is plotted against the energy. From the slopes, the Urbach energy E_U is plotted. The reference sample with only C_{60} has no PbS NCs.

Table 2. Short-Circuit Current, Open-Circuit Voltage, and Urbach Energy for Different Ligands

COINs	j_{SC} (mA/cm^2)	V_{OC} (V)	E_U (meV)
EDT	−3.03	0.09	44.8
Zn4APc	−1.53	0.06	28.3
mixed	−3.80	0.16	25.8
only C_{60}	−0.91	0.39	n.d.

strategy to improve their electrical transport properties is the use of short bidentate ligands, like EDT, forming a cross-linked NC assembly.[2] However, due to the large shrinkage of interparticle distances required to form such a structure, the particle alignment is highly irregular and accompanied by the formation of many voids and defects on the monolayer level, as confirmed in the present study as well. Additionally, defect states are formed, probably due to the rather ill-defined structural properties of the individual NC itself after ligand exchange as well as their arrangement in the film.

Therefore, the use of conjugated organic linker molecules, i.e., organic semiconductors, offers an alternative way of achieving dense solid films with better defined structural and electronic properties.[24] In particular, it has been shown that long-range ordered, crack-free solids can be achieved using relatively large organic semiconducting molecules with (one or both of) their frontier orbitals being in resonance with the NC's energy levels such that efficient charge transport is enabled despite their larger interparticle distances.[11,40,41]

Motivated by these observations, specifically the successful demonstration of superlattice formation between PbS NCs and a copper-phthalocyanine derivative,[24] we have tried to implement Zn4APc as a conjugated linker molecule in such COINs. It has a similar size as the native OA ligands such that volume shrinkage is not expected to be an issue. Surprisingly, however, all our experiments—be it transmission electron microscopy, photoelectron spectroscopy, or charge transport and photocurrent studies—point to the absence of sufficient binding of the Zn4APc ligand to replace the OA shell of NCs.

Only when a mixture of EDT and Zn4APc molecules in solution is used for the ligand exchange, we find clear evidence for the presence of the latter in the resulting COINs. As evident from the STEM images, the structure of these mixed COINs is distinctly different from both the original OA-capped PbS NCs before ligand exchange as well as the EDT-exchanged PbS NC ones. Although the structural arrangement of the mixed ligand system lacks long-range order, one can speculate that it may further be improved if instead of the dip-coating process used here, a slower film formation procedure is implemented, as demonstrated, e.g., for COIN formation at a liquid–air interface.[24] Photoelectron spectroscopy indicates and electrical transport measurements prove that a conducting network similar to the EDT case is formed, though with a significantly lower electrical conductivity.

Nevertheless, within the framework of Taube's concept of inner and outer sphere electron transfer,[42] real "through-bond" inner sphere transfer in solids of quantum dots/organic pi-systems is difficult to prove and may not have been unambiguously demonstrated to date. While some examples[11,40,41] suggest that the utilization of conjugated pi-systems leads to charge mobilities, which are larger than the expected "through-space" mobilities for a given average interparticle distance, it has been suggested that this could also be the result of percolative pathways forming via occasional shorter interparticle spacings. This is an ongoing debate. We believe that there is no fundamental reason why the utilization of organic pi-systems as "molecular wires" in quantum dot solids should not—in theory—work as well as for the individual, tailored nanocontacts with defined binding geometries.[43] In fact, optical experiments have already demonstrated this for quantum dots in solution.[44] It is therefore more a question if the field has already reached the necessary precision in the assembly of quantum dots in the solid state that would be required to maintain a favorable binding geometry for the majority of the quantum dots in the ensemble.

Most remarkably, these mixed COINs show significantly improved electro-optical properties. In addition to the excitonic absorption band of the PbS NCs itself, which is found in the near-infrared region for the used particle size, there is a clear fingerprint of the Zn4APc ligand absorption between 600 and 800 nm. Moreover, the shape of this spectrum indicates that the ligands do not aggregate, as it is often observed in phthalocyanines, which in turn is a hint for binding to PbS NCs.[45] This is confirmed by the behavior of the mixed COINs as active layers in a hybrid NC-organic solar cell. As compared to EDT and the neat Zn4APc ligand COINs, the mixed ligand system has the highest overall photocurrent and photovoltage. Furthermore, the spectral photocurrent, i.e., the incident-photon-to-current conversion efficiency, reveals contributions by all constituents of the system: PbS NCs, the Zn4APc ligand, and the C_{60} fullerene acceptor. And, as in the case of the optical absorption, the contribution of the mixed ligand device is well structured without any sign of aggregation. By contrast, the IPCE spectrum of the neat Zn4APc ligand COINs has the characteristic broad double-peak structure of aggregated phthalocyanine, which could indicate that the ligands in this case are not bound to PbS but somehow intercalated between individual NC layers or simply forming a segregated layer on top of them. This notion seems to confirm all of our observations, which lead us to the conclusion that attachment of the Zn4APc ligands to PbS NCs, forming the

desired COINs, only occurs if it is assisted by the presence of the strongly binding EDT ligand.

It is apparent that for the neat Zn4APc-ligand-exchanged sample, the absorption is significantly lower (more than 50% at 400 nm and also at the wavelength of the excitonic peak at 1150 nm) than for the other two samples, in spite of the fact that comparable film thicknesses were used. This may give a hint that in the absence of EDT, a considerable amount of PbS NCs are simply washed away and the voids are filled up with Zn4APc ligands that form aggregates among each other but do not bind to PbS. This is consistent with the observed signature of agglomeration discussed in the context of the photocurrent spectra (Figure 6c). This in turn would indicate that if EDT is added to the ligand solution, it acts primarily to immobilize PbS NCs, e.g., by pinning them to the substrate surface, so that the Zn4APc ligand has more time to find preferential binding sites. The photocurrent spectra (Figure 6c) seem to confirm this notion because the signal of the ligand is now blue-shifted and does no longer indicate aggregation but rather has the characteristic fingerprints of the Zn4APc ligand.

Finally, the electronic structure of different COINs deserves some discussion. For the calculation of the $1S_e$ level of different COINs (see Table 1), an optical gap of 1.13 eV (corresponding to the native PbS NC absorption in solution at 1090 nm) and identical exciton binding energies were used (eq 1). However, regarding the largely different dielectric permittivity of bulk PbS $(169)^{30}$ and organic ligand molecules (2...4; at the lower end for OA and in the range 3–4 for organic semiconductors), as well as their different packing and interparticle distances lead to different effective dielectric permittivity. One method to measure the dielectric function is by ellipsometry.[46] A second method, which is used here, is the effective medium approach. In an effective-medium approach, e.g., by Maxwell and Garnett,[47] this quantity is given by

$$\epsilon_{eff} = \epsilon_m \frac{\epsilon_{NC}(1 + 2\theta) - 2\epsilon_m(\theta - 1)}{\epsilon_m(2 + \theta) + \epsilon_{NC}(1 - \theta)} \qquad (2)$$

where ϵ_m and ϵ_{NC} are the dielectric permittivities of the ligand matrix and PbS NCs, respectively, and θ is the fraction of volume filled with NCs.

The volume fraction θ for different COINs is estimated from the interparticle distances and their radii. Thereby, we assume that voids or larger uncovered areas seen for monolayers of the STEM samples will be filled by NCs in thicker multilayer structures preserving the same average distances in the third spatial dimension as well. Thus, θ will be highest for EDT owing to the very close interparticle distances and lowest for the native OA-capped NC arrangement. The neat Zn4APc COINS are similar to the native case, whereas the mixed COINs are intermediate. Under these assumptions, a qualitative scenario of the resulting effective-medium permittivities is shown in Figure 7.

According to eq 1, this has consequences for the apparent optical gap of different COINs, as the exciton binding energy depends on the (effective) dielectric constant of the quantum dot. Thus, if the estimated ϵ_m's from Figure 7 are used, one obtains a shift in the optical gaps (as compared to the native NCs in solution with a value of 1.13 eV) of about 0.17 eV for OA ($\epsilon_{eff} \approx 8.2$, $\epsilon_m \approx 2$), 0.08 eV for EDT ($\epsilon_{eff} \approx 18.5$, $\epsilon_m \approx 2.2^{30}$), 0.11 eV for neat Zn4APc ($\epsilon_{eff} \approx 12.7$, $\epsilon_m \approx 3$), and 0.09 eV for mixed COINs ($\epsilon_{eff} \approx 16.3$, $\epsilon_m \approx 3$). This effect is visible in both the optical absorption measurements shown in Figure
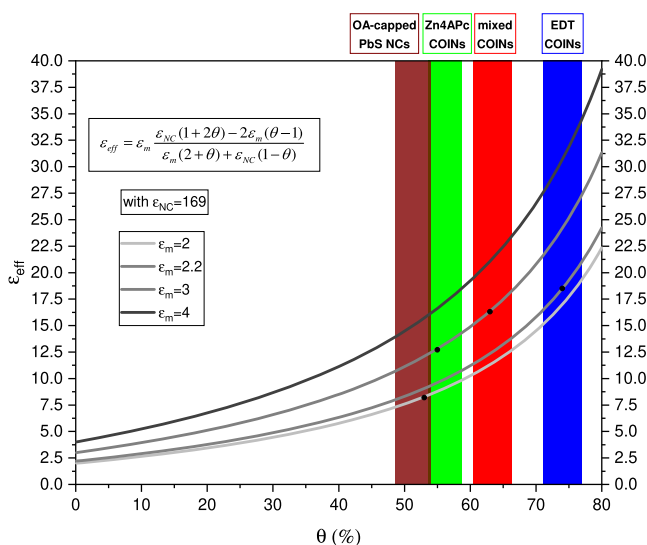
Figure 7. Change of the effective permittivity by changing the fraction of the volume filled for different optical permittivities. The colored areas give an estimated value for the fraction of the volume filled for different COINs. The dots indicate the estimated effective values for different ligands. The value for EDT COINs is taken from Bozyigi et al.[30]

3 and the photocurrent spectra of Figure 6, although not quantitatively because there is an additional small shift already from solution to thin films of about 0.02 eV. Thus, the observed shift of the PbS NC absorption peak is mainly attributed to a change in the permittivity of the effective medium surrounding the NCs.[48] It induces a change in the electronic coupling among the neighboring NCs.[49] Further, a broadening of the spectra and a redshift can be additionally caused by increased energetic/structural disorder in the film due to the ligand exchange process.[50] Another reason for the shift can be an increase of the ligand concentration of the PbS NC film.[51]

4. CONCLUSIONS

In summary, we have successfully fabricated COINs of PbS NCs and mixed organic linker molecules. The focus was to understand the mechanism of binding of different ligands. Thereby, the short, strongly binding EDT ligand was used to assist attachment of the conjugated organic semiconductor Zn4APc to achieve sufficient binding to the PbS NCs. These mixed ligand COINs exhibit superior film quality as well as improved photo-electrical behavior, such as higher photovoltage and photocurrent. The electronic properties of different COINs are consistently explained by an effective-medium approximation based on their different bindings and the resulting structural arrangements. We anticipate that the mixing of linker molecules may significantly widen the application perspectives of covalently coupled organic–inorganic nanostructures.

■ AUTHOR INFORMATION

Corresponding Author

Wolfgang Brütting − *Institut für Physik, Universität Augsburg, 86135 Augsburg, Germany;* orcid.org/0000-0001-9895-8281; Email: wolfgang.bruetting@physik.uni-augsburg.de.

Authors

Florian Grassl − *Institut für Physik, Universität Augsburg, 86135 Augsburg, Germany*

Aladin Ullrich − *Institut für Physik, Universität Augsburg, 86135 Augsburg, Germany*

Ahmed E. Mansour − *Institut für Physik & IRIS Adlershof, Humboldt-Universität zu Berlin, 12489 Berlin, Germany; Helmholtz-Zentrum Berlin für Materialien und Energie GmbH, 12489 Berlin, Germany*

Shaimaa M. Abdalbaqi − *Institut für Physik, Universität Augsburg, 86135 Augsburg, Germany*

Norbert Koch − *Institut für Physik & IRIS Adlershof, Humboldt-Universität zu Berlin, 12489 Berlin, Germany; Helmholtz-Zentrum Berlin für Materialien und Energie GmbH, 12489 Berlin, Germany;* orcid.org/0000-0002-6042-6447

Andreas Opitz − *Institut für Physik & IRIS Adlershof, Humboldt-Universität zu Berlin, 12489 Berlin, Germany;* orcid.org/0000-0002-3214-8398

Marcus Scheele − *Institut für Physikalische und Theoretische Chemie, Universität Tübingen, 72076 Tübingen, Germany;* orcid.org/0000-0002-2704-3591

Notes

The authors declare no competing financial interest.

■ REFERENCES

(1) Scheele, M. Briding the Gap: Where Inorganic Quantum Dots and Organic Semiconductors Meet. *Bunsenmagazin* **2014**, *4*, 168−175.

(2) Liu, Y.; Gibbs, M.; Puthussery, J.; Gaik, S.; Ihly, R.; Hilhouse, H.; Law, M. Dependence of Carrier Mobility on Nanocrystal Size and Ligand Length in PbSe Nanocrystal Solids. *Nano Lett.* **2010**, *10*, 1960−1969.

(3) Zhitomirsky, D.; Voznyy, O.; Hoogland, S.; Sargent, E. H. Measuring Charge Carrier Diffusion in Coupled Colloidal Quantum Dot Solids. *ACS Nano* **2013**, *7*, 5282−5290.

(4) Brown, P. R.; Kim, D.; Lunt, R. R.; Zhao, N.; Bawendi, M. G.; Grossman, J. C.; Bulovic, V. Energy Level Modification in Lead Sulfide Quantum Dot Thin Films through Ligand Exchange. *ACS Nano* **2014**, *8*, 5863−5872.

(5) Luther, J. M.; Law, M.; Beard, M. C.; Song, Q.; Reese, M. O.; Ellingson, R. J.; Nozik, A. J. Schottky Solar Cells Based on Colloidal Nanocrystal Films. *Nano Lett.* **2008**, *8*, 3488−3492.

(6) Alivisatos, A. Semiconductor Clusters, Nanocrystals, and Quantum Dots. *Science* **1996**, *271*, 933−937.

(7) Maraghechi, P.; Labelle, A. J.; Kirmani, A. R.; Lan, X.; Adachi, M. M.; Thon, S. M.; Hoogland, S.; Lee, A.; Ning, Z.; Fischer, A.;

Amassian, A.; Sargent, E. H. The Donor-Supply Electrode Enhances Performance in Colloidal Quantum Dot Solar Cells. *ACS Nano* **2013**, *7*, 6111−6116.

(8) Nozik, A. J. Quantum Dot Solar Cells. *Phys. E* **2002**, *14*, 115−120.

(9) Scheele, M.; Brütting, W.; Schreiber, F. Coupled Organic-Inorganic Nanostructures (COIN). *Phys. Chem. Chem. Phys.* **2015**, *17*, 97−111.

(10) Chung, D. S.; Lee, J.-S.; Huang, J.; Nag, A.; Ithurria, S.; Talapin, D. V. Low Voltage, Hysteresis Free, and High Mobility Transistors from All-Inorganic Colloidal Nanocrystals. *Nano Lett.* **2012**, *12*, 1813−1820.

(11) André, A.; Zherebetskyy, D.; Hanifi, D.; He, B.; Samadi Khoshkhoo, M.; Jankowski, M.; Chasseé, T.; Wang, L.-W.; Schreiber, F.; Salleo, A.; Liu, Y.; Scheele, M. Toward Conductive Mesocrystalline Assemblies: PbS Nanocrystals Cross-Linked with Tetrathiafulvalene Dicarboxylate. *Chem. Mater.* **2015**, *27*, 8105−8115.

(12) Lan, X.; Voznyy, O.; García de Arquer, F. P.; Liu, M.; Xu, J.; Proppe, A. H.; Walters, G.; Fan, F.; Tan, H.; Liu, M.; Yang, Z.; Hoogland, S.; Sargent, E. H. 10.6% Certified Colloidal Quantum Dot Solar Cells via Solvent-Polarity-Engineered Halide Passivation. *Nano Lett.* **2016**, *16*, 4630−4634.

(13) Weidman, M. C.; Yager, K. G.; Tisdale, W. A. Interparticle Spacing and Structural Ordering in Superlattice PbS Nanocrystal Solids Undergoing Ligand Exchange. *Chem. Mater.* **2015**, *27*, 474−482.

(14) Lauth, J.; Grimaldi, G.; Kinge, S.; Houtepen, A. J.; Siebbeles, L. D.; Scheele, M. Ultrafast Charge Transfer and Upconversion in Zinc β-Tetraaminophthalocyanine-Functionalized PbS Nanostructures Probed by Transient Absorption Spectroscopy. *Angew. Chem., Int. Ed.* **2017**, *56*, 14061−14065.

(15) Jung, S.-H.; Choi, J.-H.; Yang, S.-M.; Cho, W.-J.; Ha, C.-S. Syntheses and Characterization of Soluble Phthalocyanine Derivatives for Organic Electroluminescent Devices. *Mate. Sci. Eng. B* **2001**, *85*, 160−164.

(16) Kim, B.-S.; Hong, J.; Hou, B.; Cho, Y.; Sohn, J. I.; Cha, S.; Kim, J. M. Inorganic-Ligand Exchanging Time Effect in PbS Quantum Dot Solar Cell. *Appl. Phys. Lett.* **2016**, *109*, No. 063901.

(17) Tang, J.; Kemp, K. W.; Hoogland, S.; Jeong, K. S.; Liu, H.; Levina, L.; Furukawa, M.; Wang, X.; Debnath, R.; Cha, D.; Chou, K. W.; Fischer, A.; Amassian, A.; Asbury, J. B.; Sargent, E. H. Colloidal-Quantum-Dot Photovoltaics Using Atomic-Ligand Passivation. *Nat. Mater.* **2011**, *10*, 765−771.

(18) Harder, E.; Damm, W.; Maple, J.; Wu, C.; Reboul, M.; Xiang, J.; Wang, L.; Lupyan, D.; Dahlgren, M.; Knight, J.; Kaus, J.; Cerutti, D.; Krilov, G.; Jorgensen, W.; Abel, R.; Friesner, R. OPLS3: a Force Field Providing Broad Coverage of Drug-Like Small Molecules and Proteins. *J. Chem. Theory Comput.* **2016**, *12*, 281−296.

(19) Schrödinger Release 2019-4: Materials Science Suite, Schrödinger, LLC, New York, NY. www.schrodinger.com., 2019.

(20) Luther, J. M.; Law, M.; Song, Q.; Perkins, C. L.; Beard, M. C.; Nozik, A. J. Structural, Optical, and Electrical Properties of Self-Assembled Films of PbSe Nanocrystals Treated with 1, 2-Ethanedithiol. *ACS Nano* **2008**, *2*, 271−280.

(21) Ehrler, B.; Wilson, M. W.; Rao, A.; Friend, R. H.; Greenham, N. C. Singlet Exciton Fission-Sensitized Infrared Quantum Dot Solar Cells. *Nano Lett.* **2012**, *12*, 1053−1057.

(22) Pradhan, N.; Reifsnyder, D.; Xie, R.; Aldana, J.; Peng, X. Surface Ligand Dynamics in Growth of Nanocrystals. *J. Am. Chem. Soc.* **2007**, *129*, 9500−9509.

(23) Moreels, I.; Justo, Y.; de Geyter, B.; Haustraete, K.; Martins, J. C.; Hens, Z. Size-Tunable, Bright, and Stable PbS Quantum Dots: A Surface Chemistry Study. *ACS Nano* **2011**, *5*, 2004−2012.

(24) André, A.; Theurer, C.; Lauth, J.; Maiti, S.; Hodas, M.; Khoshkhoo, M. S.; Kinge, S.; Meixner, A.; Schreiber, F.; Siebbeles, L.; Braun, K.; Scheele, M. Structure, Transport and Photoconductance of PbS Quantum Dot Monolayers Functionalized with a Copper Phthalocyanine Derivative. *Chem. Commun.* **2017**, *53*, 1700−1703.

(25) Choi, J. J.; Luria, J.; Hyun, B.-R.; Bartnik, A. C.; Sun, L.; Lim, Y.-F.; Marohn, J. A.; Wise, F. W.; Hanrath, T. Photogenerated Exciton Dissociation in Highly Coupled Lead Salt Nanocrystal Assemblies. *Nano Lett.* **2010**, *10*, 1805−1811.

(26) Novák, J.; Banerjee, R.; Kornowski, A.; Jankowski, M.; André, A.; Weller, H.; Schreiber, F.; Scheele, M. Site-Specific Ligand Interactions Favor the Tetragonal Distortion of PbS Nanocrystal Superlattices. *ACS Appl. Mater. Interfaces* **2016**, *8*, 22526−22533.

(27) Moreels, I.; Lambert, K.; Smeets, D.; de Muynck, D.; Nollet, T.; Martins, J. C.; Vanhaecke, F.; Vantomme, A.; Delerue, C.; Allan, G.; Hens, Z. Size-Dependent Optical Properties of Colloidal PbS Quantum Dots. *ACS Nano* **2009**, *3*, 3023−3030.

(28) Schultz, T.; Lenz, T.; Kotadiya, N.; Heimel, G.; Glasser, G.; Berger, R.; Blom, P. W.; Amsalem, P.; de Leeuw, D. M.; Koch, N. Reliable Work Function Determination of Multicomponent Surfaces and Interfaces: The Role of Electrostatic Potentials in Ultraviolet Photoelectron Spectroscopy. *Adv. Mater. Interfaces* **2017**, *4*, No. 1700324.

(29) Jasieniak, J.; Califano, M.; Watkins, S. Size-Dependent Valence and Conduction Band-Edge Energies of Semiconductor Nanocrystals. *ACS Nano* **2011**, *5*, 5888−5902.

(30) Bozyigit, D.; Wood, V. Electrical Characterization of Nanocrystal Solids. *J. Mater. Chem. C* **2014**, *2*, 3172−3184.

(31) Steiner, A. M.; Lissel, F.; Fery, A.; Lauth, J.; Scheele, M. Prospects of Coupled Organic-Inorganic Nanostructures for Charge and Energy Transfer Applications. *Angew. Chem., Int. Ed.* **2021**, *60*, 1152−1175.

(32) Knupfer, M. Exciton Binding Energies in Organic Semiconductors. *Appl. Phys. A: Mater. Sci. Process.* **2003**, *77*, 623−626.

(33) Brown, T.; Kim, J.; Friend, R.; Cacialli, F.; Daik, R.; Feast, W. Built-In Field Electroabsorption Spectroscopy of Polymer Light-Emitting Diodes Incorporating a Doped Poly(3,4-Ethylene Dioxythiophene) Hole Injection Layer. *Appl. Phys. Lett.* **1999**, *75*, 1679−1681.

(34) Wagner, J.; Gruber, M.; Wilke, A.; Tanaka, Y.; Topczak, K.; Steindamm, A.; Hörmann, U.; Opitz, A.; Nakayama, Y.; Ishii, H.; Plaum, J.; Koch, N.; Brütting, W. Identification of Different Origins for S-Shaped Current Voltage Characteristics in Planar Heterojunction Organic Solar Cells. *J. Appl. Phys.* **2012**, *111*, No. 054509.

(35) Peumans, P.; Bulović, V.; Forrest, S. R. Efficient Photon Harvesting at High Optical Intensities in Ultrathin Organic Double-Heterostructure Photovoltaic Diodes. *Appl. Phys. Lett.* **2000**, *76*, 2650−2652.

(36) Linderl, T.; Zechel, T.; Hofmann, A.; Sato, T.; Shimizu, K.; Ishii, H.; Brütting, W. Crystalline versus Amorphous Donor-Acceptor Blends: Influence of Layer Morphology on the Charge-Transfer Density of States. *Phys. Rev. Appl.* **2020**, *13*, No. 024061.

(37) Urbach, F. The Long-Wavelength Edge of Photographic Sensitivity and of the Electronic Absorption of Solids. *Phys. Rev.* **1953**, *92*, 1324.

(38) Erslev, P. T.; Chen, H.-Y.; Gao, J.; Beard, M. C.; Frank, A. J.; van de Lagemaat, J.; Johnson, J. C.; Luther, J. M. Sharp Exponential Band Tails in Highly Disordered Lead Sulfide Quantum Dot Arrays. *Phys. Rev. B* **2012**, *86*, No. 155313.

(39) Heuer-Jungemann, A.; Feliu, N.; Bakaimi, I.; Hamaly, M.; Alkilany, A.; Chakraborty, I.; Masood, A.; Casula, M.; Kostopoulou, A.; Oh, E.; Susumu, K.; Stewart, M.; Medintz, I.; Stratakis, E.; Parak, W.; Kanaras, A. The Role of Ligands in the Chemical Synthesis and Applications of Inorganic Nanoparticles. *Chem. Rev.* **2019**, *119*, 4819−4880.

(40) André, A.; Weber, M.; Wurst, K. M.; Maiti, S.; Schreiber, F.; Scheele, M. Electron-Conducting PbS Nanocrystal Superlattices with Long-Range Order Enabled by Terthiophene Molecular Linkers. *ACS Appl. Mater. Interfaces* **2018**, *10*, 24708−24714.

(41) Scheele, M.; Hanifi, D.; Zherebetskyy, D.; Chourou, S. T.; Axnanda, S.; Rancatore, B. J.; Thorkelsson, K.; Xu, T.; Liu, Z.; Wang, L.-W.; Liu, Y.; Alivisatos, A. P. PbS Nanoparticles Capped with Tetrathiafulvalenetetracarboxylate: Utilizing Energy Level Alignment for Efficient Carrier Transport. *ACS Nano* **2014**, *8*, 2532−2540.

(42) Creutz, C.; Ford, P. C.; Meyer, T. J. Henry Taube: Inorganic Chemist Extraordinaire. *Inorg. Chem.* **2006**, *45*, 7059−7068.

(43) Schwarz, F.; Kastlunger, G.; Lissel, F.; Riel, H.; Venkatesan, K.; Berke, H.; Stadler, R.; Lörtscher, E. High-Conductive Organometallic Molecular Wires with Delocalized Electron Systems Strongly Coupled to Metal Electrodes. *Nano Lett.* **2014**, *14*, 5932−5940.

(44) Li, X.; Fast, A.; Huang, Z.; Fishman, D. A.; Tang, M. L. Complementary Lock-and-Key Ligand Binding of a Triplet Transmitter to a Nanocrystal Photosensitizer. *Angew. Chem., Int. Ed.* **2017**, *56*, 5598−5602.

(45) Howe, L.; Zhang, J. Ultrafast Studies of Excited-State Dynamics of Phthalocyanine and Zinc Phthalocyanine Tetrasulfonate in Solution. *J. Phys. Chem. A* **1997**, *101*, 3207−3213.

(46) Diroll, B. T.; Gaulding, E. A.; Kagan, C. R.; Murray, C. B. Spectrally-Resolved Dielectric Functions of Solution-Cast Quantum Dot Thin Films. *Chem. Mater.* **2015**, *27*, 6463−6469.

(47) Scheele, M.; Engel, J. H.; Ferry, V. E.; Hanifi, D.; Liu, Y.; Alivisatos, A. P. Nonmonotonic Size Dependence in the Hole Mobility of Methoxide-Stabilized PbSe Quantum Dot Solids. *ACS Nano* **2013**, *7*, 6774−6781.

(48) Kahmann, S.; Mura, A.; Protesescu, L.; Kovalenko, M. V.; Brabec, C. J.; Loi, M. A. Opto-Electronics of PbS Quantum Dot and Narrow Bandgap Polymer Blends. *J. Mater. Chem. C* **2015**, *3*, 5499−5505.

(49) Xu, F.; Gerlein, L. F.; Ma, X.; Haughn, C. R.; Doty, M. F.; Cloutier, S. G. Impact of Different Surface Ligands on the Optical Properties of PbS Quantum Dot Solids. *Materials* **2015**, *8*, 1858−1870.

(50) Guyot-Sionnest, P. Electrical Transport in Colloidal Quantum Dot Films. *J. Phys. Chem. Lett.* **2012**, *3*, 1169−1175.

(51) Kirmani, A. R.; Walters, G.; Kim, T.; Sargent, E. H.; Amassian, A. Optimizing Solid-State Ligand Exchange for Colloidal Quantum Dot Optoelectronics: How Much Is enough. *ACS Appl. Energy Mater.* **2020**, *3*, 5385−5392.